Accuracy enhancement of digital image correlation with B-spline interpolation

Long Luu,[1,2] Zhaoyang Wang,[1,*] Minh Vo,[1,2] Thang Hoang,[1] and Jun Ma[1]

[1]*Department of Mechanical Engineering, The Catholic University of America, Washington, D.C. 20064, USA*

[2]*Department of Electrical Engineering, The Catholic University of America, Washington, D.C. 20064, USA*

*Corresponding author: wangz@cua.edu

The interpolation algorithm plays an essential role in the digital image correlation (DIC) technique for shape, deformation, and motion measurements with subpixel accuracies. At the present, little effort has been made to improve the interpolation methods used in DIC. In this Letter, a family of recursive interpolation schemes based on B-spline representation and its inverse gradient weighting version is employed to enhance the accuracy of DIC analysis. Theories are introduced, and simulation results are presented to illustrate the effectiveness of the method as compared with the common bicubic interpolation.   © 2011 Optical Society of America

OCIS codes: 120.4290, 120.6165, 100.2000, 150.1135.

Digital image correlation (DIC) [1] is a noncontact, noninterferometric optical metrology for displacement, motion, and deformation measurements. The technique works by comparing the grayscale images of an object captured at different times, stages of deformation, or views. Through tracking each pixel of interest in the reference and target images using a square subset of pixels centered at the interrogated pixel, the DIC technique can build up whole-field two-dimensional (2D) and three-dimensional (3D) deformation or motion vector fields and their gradient maps. In recent years, DIC has found numerous applications in many fields [2].

Generally, DIC uses an iterative algorithm, such as the Newton–Raphson or Levenberg–Marquardt method, to carry out the registration of subsets (i.e., matching subsets) according to a correlation criterion [3,4]. Because the smallest element in a digital image is one pixel, an interpolation process of the target image is essential for the measurement to achieve subpixel accuracies. In addition, during the analysis, the subset matching process resorts to image interpolation many times. Because there are many subsets, each containing hundreds of pixels, and the entire DIC processing takes a number of iteration cycles for each subset analysis, it is evident that a great amount of computation time in DIC is dedicated to the intensity interpolations of noninteger pixels.

One of the most commonly used interpolation methods for DIC is the bicubic interpolation, which is a robust algorithm capable of providing high accuracy at a low computational cost. Nevertheless, the ever-increasing applications of DIC in a broad range of scientific and engineering fields result in a strong demand for higher levels of accuracy. In this Letter, we will present a family of interpolation methods, which is based on B-spline functions. Since the first application of the B-spline interpolation in image processing by Hou and Andrews [5], much progress has been made by the digital filter approach proposed by Unser *et al.* [6]. Owing to their work, one can now implement the B-spline interpolation prefiltering using recurrence relation, which greatly improves the calculation speed compared with the matrix approach in [5]. Figure 1 illustrates a general procedure of the B-spline interpolation. The gain factor G and the

pole z_k come from the derivation of the digital filter form of B-spline interpolation, and K is the order of the B-spline function [6].

Since the work of Unser *et al.* [6,7], many other modifications have been suggested to further improve the accuracy of B-spline interpolation. For instance, in [8] an approximation theory is used to minimize the asymptotic approximation constant and, accordingly, minimize the interpolation error. From the analytical solution proposed in [8], we can design the prefilter and postfilter for B-spline interpolation as it is done for the classical B-spline [6]. For the case of the cubic optimal maximal-order-minimal-support (O-MOMS) algorithm, the all-pole prefilter assumes the form

$$-\frac{21z_1}{4}\frac{1}{(1-z_1z)(1-z_1z^{-1})},\qquad(1)$$

where $z_1 = (-13 + \sqrt{105})/8$ is the pole and the gain factor is $-21z_1/4$. The corresponding impulse response of the postfilter can be written as

$$\beta^3(x) = \begin{cases} \frac{|x|^3}{2} - x^2 + \frac{|x|}{14} + \frac{13}{21}, & 0 \le |x| \le 1 \\ -\frac{|x|^3}{6} + x^2 - \frac{85}{42}|x| + \frac{29}{11}, & 1 \le |x| \le 2 \\ 0, & \text{otherwise} \end{cases}\qquad(2)$$

Like the above cubic algorithm, higher order O-MOMS algorithms can be obtained in a similar manner. One can refer to [7] for a similar implementation procedure of the pre- and postfilters.

Gotchev *et al.* presented a variation of the B-spline by linearly combining the B-spline function with its lower order counterparts [9]. This variation, named the modified
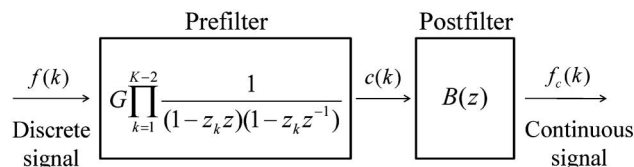

Fig. 1.   Block diagram of B-spline interpolation.

cubic B-spline, has also been incorporated into the simulation and comparison.

Another notable technique named the inverse gradient weighting initially introduced for bicubic interpolation [10] is also extended and incorporated here into the family of B-spline interpolation. Generally, because all the convolution-based interpolations tend to smooth out the data at the steep edge of the image, this modification will enhance the performance of the interpolation at those points owing to the approximation of the image gradient. The inverse gradient weighting factors in one dimension are

$$
\begin{aligned}
H_l &= \frac{1}{\sqrt{1+a|f_i-f_{i-1}|}} \\
H_r &= \frac{1}{\sqrt{1+a|f_{i+2}-f_{i+1}|}} \quad , \\
D &= H_l(1-s) + H_r s
\end{aligned}
\tag{3}
$$

where f_i is the intensity level of pixel i, s is the subpixel location with the origin at pixel i, and a is the sharpness factor. For the case of linear interpolation with the convolution kernel (w_0, w_1), where $w_0 = 1 - s$ and $w_1 = s$, the modified coefficients become $w_0 = H_l(1-s)/D$ and $w_1 = H_r s/D$. This modification can be directly extended to the 2D case for other interpolation kernels of higher orders [10].

To investigate the performance and accuracy of the B-spline interpolation in the DIC analysis, numerical experiments have been carried out using computer-generated images. The reason for the use of simulated images instead of real experimental images is that it can provide controlled displacements of exact values for accuracy examination purpose and can eliminate errors caused by the image acquisition system, imperfect loading, and other uncertainties to avoid clouding the error associated with interpolation. The equations used to generate the images to be tested by the DIC algorithm are [11]

Fig. 2.   RMSE of displacements obtained by using various interpolation algorithms.

$$
\begin{aligned}
I_r(x,y) &= \sum_{k=1}^{n} A_k \exp(-((x-x_k)^2 + (y-y_k)^2)/R^2) \\
I_t(x,y) &= \sum_{k=1}^{n} A_k \exp(-((x-x_k-u_0-u_x x-u_y y)^2 + (y-y_k-v_0-v_x x-v_y y)^2)/R^2)
\end{aligned}
\tag{4}
$$

where n is the number of granules in the image; R is the feature size of the granules; (x_k, y_k) and A_k are random positions and intensity levels of the granules; u_0, v_0, u_x, u_y, v_x, and v_y are deformation parameters; and I_r and I_t are the intensity levels at pixel (x, y) in the reference and target images, respectively. In image generation, we set $n = 2500$, $R = 3$, the image size is set to 300×300 pixels, and the grayscale quantization is set to 16 bits. In the DIC analysis, we use a subset size of 31×31 pixels, a simple yet robust correlation criterion named the parametric sum of squared difference (PSSD_{ab}) [3], and the classic Newton–Raphson algorithm [2] for subset matching.

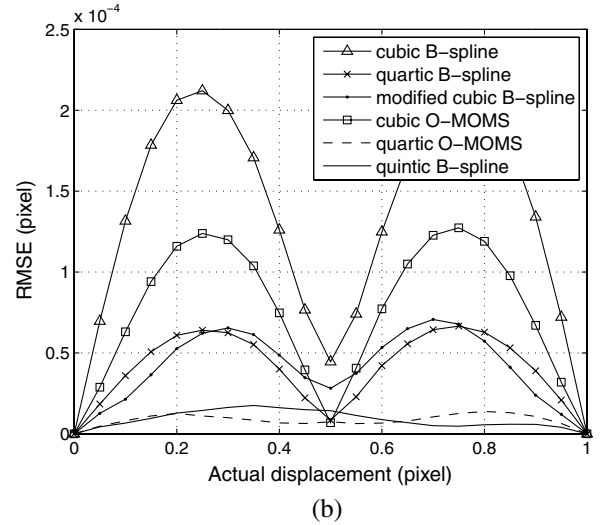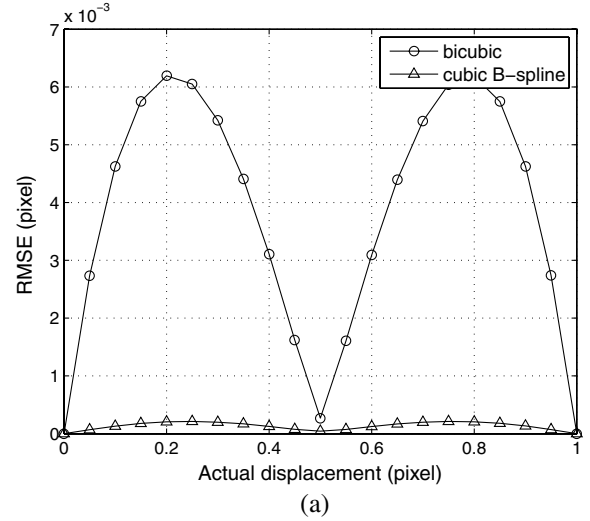In the first numerical experiment, we simulated the successive rigid-body translation by assigning 0 to 1 pixel to u_0 with an increment of 0.05 pixel and setting the other parameters to zeros. Figure 2 shows the root-mean-squared error (RMSE) obtained by different interpolation algorithms for each displacement. For clarification, the data have been separated into two subfigures with the same cubic B-spline results shown in both. It is evident that the family of B-spline interpolation yields much better results than the bicubic one. Particularly, the quartic O-MOMS algorithm and the quintic B-spline algorithm yield the highest accuracies, which are hundreds of times better than the accuracy provided by the bicubic algorithm with respect to the RMSE.

In the second simulation, we take into account all of the deforming parameters with the following representative
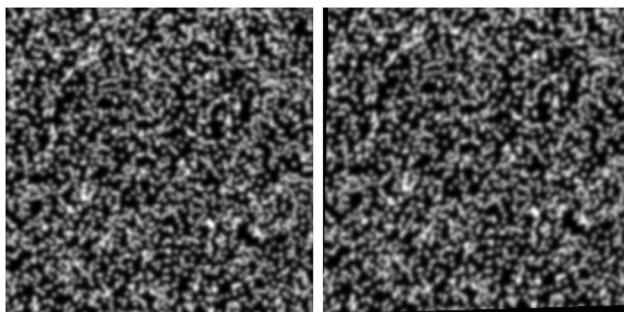
Fig. 3.   Reference and deformed images.

values: $u_0 = 10.25$, $u_x = 0.01$, $u_y = 0.02$, $v_0 = 5.75$, $v_x = 0.03$, and $v_y = 0.04$. The images are shown in Fig. 3. The RMSEs are summarized in Table 1. It is clearly verified that the B-spline interpolation functions are superior to the bicubic algorithm.

The aforementioned two numerical experiments are conducted with the inverse gradient weighting approach of the B-spline interpolation. Because of page limitations, only the special case $a = 0$, which corresponds to the normal B-spline interpolation, has been presented.

To demonstrate the validity of the inverse gradient weighting scheme, Fig. 4 shows a representative result from the first simulation, where the data are obtained by the cubic B-spline interpolation with various values of the inverse gradient weighting coefficient a. It can be seen from the figure that a decrease in the value of a yields a higher accuracy for most displacements but causes worse results at the two ends of the investigated displacements, i.e., 0, 0.05, 0.95 and 1 pixel. An appropriate selection of coefficient a can help enhance the accuracy of the B-spline family of interpolation. From the analysis of a number of numerical images with various contrasts, it is found that the same trend holds and the value of a around -3.0×10^{-5} is recommended for the best trade-off between the errors of the displacement at the two ends and those otherwise. The same result is observed for other B-spline functions as well. It is noteworthy that a is chosen from the simulation results, not from analytical calculation.

By means of the recursive implementation, the computation speed of the B-spline interpolation is almost equivalent to that of the bicubic interpolation in the presented numerical experiments. This agrees with the results reported in other literatures [6,7].

Table 1.   RMSE Yielded by Various Interpolation Algorithms for Displacements with Large Shear Strains

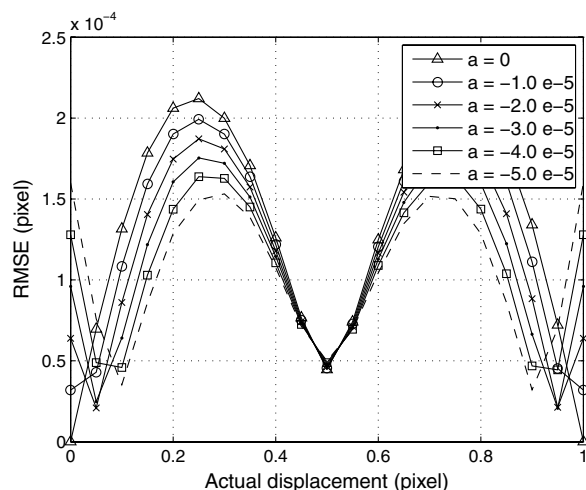| Interpolation Algorithm	RMSE (Pixel)	
	u	v
Bicubic	1.881×10^{-3}	7.199×10^{-4}
Cubic B-spline	7.666×10^{-5}	4.933×10^{-5}
Quartic B-spline	2.093×10^{-5}	1.135×10^{-5}
Modified cubic B-spline	3.809×10^{-5}	3.399×10^{-5}
Cubic O-MOMS	3.759×10^{-5}	1.943×10^{-5}
Quartic O-MOMS	6.657×10^{-6}	5.719×10^{-6}
Quintic B-spline	1.062×10^{-5}	7.965×10^{-6}

Fig. 4.   RMSE of displacements obtained by using inverse gradient weighting version of the cubic B-spline.

Because of the nature of the B-spline interpolation, which consists of a prefilter acting as a high-pass filter, the noise encountered in real-world applications can substantially affect the accuracies of the corresponding DIC analysis. For instance, when random noise with an amplitude up to 0.5% of the maximum intensity of the pattern is added to every pixel in the reference and deformed images in the second simulation, the RMSEs associated with the bicubic algorithm change slightly to 1.927×10^{-3} and 8.450×10^{-4}, for u and v displacements, respectively, whereas the errors from all the B-spline algorithms increase to similar values ranging from $4.058 \times 10^{-4} \sim 4.125 \times 10^{-4}$ for u displacement and $4.288 \times 10^{-4} \sim 4.534 \times 10^{-4}$ for v displacement. For this reason, in addition to using accurate interpolation algorithms, it is highly demanded in DIC applications to use a high-pixel-depth, high-quality imaging system.

References
1. W. Sharpe, *Handbook of Experimental Solid Mechanics* (Springer, 2008).
2. M. Sutton, J. Orteu, and H. Schreier, *Image Correlation for Shape, Motion and Deformation Measurements* (Springer, 2009).
3. B. Pan, H. Xie, and Z. Wang, Appl. Opt. **49**, 5501 (2010).
4. W. Tong, Opt. Lett. **36**, 763 (2011).
5. H. Hou and H. Andrews, IEEE Trans. Acoust. Speech Signal Process. **26**, 508 (1978).
6. M. Unser, A. Aldroubi, and M. Eden, IEEE Trans. Pattern Anal. Mach. Intell. **13**, 277 (1991).
7. M. Unser, IEEE Signal Proc. Mag. **16** (6), 22 (1999).
8. T. Blu, P. Thevenaz, and M. Unser, IEEE Trans. Image Process. **10**, 1069 (2001).
9. A. Gotchev, K. Egiazarian, J. Vesma, and T. Saramaki, in *Proceedings of the IEEE International Conference on Acoustics, Speech, and Signal Processing*, Vol. 3 (IEEE, 2001), pp. 1865–1868.
10. J. Hwang and H. Lee, IEEE Signal Process. Lett. **11**, 359 (2004).
11. B. Pan, H. Xie, B. Xu, and F. Dai, Meas. Sci. Technol. **17**, 1615 (2006).